



HAL
open science

Ridgelet Decomposition: Discrete Implementation and Color Denoising

Philippe Carré, David Helbert

► **To cite this version:**

Philippe Carré, David Helbert. Ridgelet Decomposition: Discrete Implementation and Color Denoising. Wavelet Applications in Industrial Processing III, Oct 2005, Boston, MA, United States. 10.1117/12.629569 . hal-00331496

HAL Id: hal-00331496

<https://hal.science/hal-00331496>

Submitted on 4 Apr 2023

HAL is a multi-disciplinary open access archive for the deposit and dissemination of scientific research documents, whether they are published or not. The documents may come from teaching and research institutions in France or abroad, or from public or private research centers.

L'archive ouverte pluridisciplinaire **HAL**, est destinée au dépôt et à la diffusion de documents scientifiques de niveau recherche, publiés ou non, émanant des établissements d'enseignement et de recherche français ou étrangers, des laboratoires publics ou privés.

Ridgelet Decomposition: Discrete implementation and Color denoising

Philippe Carré and David Helbert

SIC Laboratory - FRE-CNRS 2731 University of Poitiers - UFR Sciences -SP2MI
Boulevard Marie et Pierre Curie Teleport 2 BP 30179 86962 Futuroscope Chasseneuil CEDEX
France

ABSTRACT

In this paper, we review an implementation of the Ridgelet transform: The Discrete Analytical Ridgelet Transform (DART). This transform uses the Fourier strategy for the computation of the associated 2-D and 3-D discrete Radon transforms. The innovative step is the definition of a **discrete** 3-D transform and the construction of discrete analytical lines in the Fourier domain. These discrete analytical lines have a parameter called arithmetical thickness, allowing us to define a DART adapted to a specific application. Indeed, the DART representation is not orthogonal, It is associated with a flexible redundancy factor.

The DART has a very simple forward/inverse algorithm that provides an exact reconstruction without any iterative method. We had proved in different publications that the 2D and 3D DART are performant for the level of greys images restorations. Therefore we have interesting to 2D/3D color image restoration. We have compared the restoration results in function of different color space definition and importance of the white Gaussian noise. We criticize our results with two different measures : the Signal Noise Ratio calculation and perceptual measures to evaluate the perceptual colour difference between original and denoised images. These experimental results show that the simple thresholding of the DART coefficients is competitive than the classical denoising techniques.

Keywords: Ridgelet Transform, Discrete Analytical Lines, Denoising, Color images

1. INTRODUCTION

A team of Stanford has recently developed an alternative system of multiresolution analysis, called Ridgelet, specifically designed to efficiently represent edges in images.¹ The Ridgelet transform can be computed by performing a wavelet analysis in the Radon domain. However, most of the work done with Ridgelets has been theoretical in nature. To our knowledge, we can find in the literature only two main implementations for the discrete Ridgelet decomposition.^{2,3} This paper reviews a new approach that aims at representing linear singularities with a discrete Ridgelet transform based on discrete analytical lines: the Discrete Analytical Ridgelet Transform (DART). The idea behind the associated discrete Radon transform is to define each Radon projection by a discrete analytical line in the Fourier domain. There are several advantages at using discrete analytical lines: they offer a theoretical framework for the definition of the discrete Radon projections. This solution allows us to have different Ridgelet decompositions according to the arithmetical thickness of the discrete lines (control of the redundancy factor, i.e. $\frac{\text{number of transform coefficients}}{\text{number of image pixels}}$, of the transform). The DART has a very simple and rapid forward/inverse algorithm. This simple straightforward approach ensures an exact reconstruction without interpolation nor iterative process. Moreover, the objects defined in discrete analytical geometry (3D lines, planes, hyperplanes, ...) allows simple extensions to 3D and even higher dimensions. In order to compare the performances of the DART, we have compared the restoration results in function of different importance of the white Gaussian noise.

Further author information: (Send correspondence to P. Carré)
E-mail: carre@sic.sp2mi.univ-poitiers.fr

2. THE 2-D RIDGELET TRANSFORM

2.1. Continuous theory of Ridgelet transform

A substantial foundation for Ridgelet analysis is documented in the Ph.D. thesis of Candès.¹ The continuous Ridgelet transform of $s \in L^2(\mathbb{R}^2)$ is defined as the scalar product of s with a function $\psi_{a,b,\theta}$ the Ridgelet 2-D function defined from a wavelet 1-D function ψ as:

$$\psi_{a,b,\theta}(\mathbf{x}) = a^{-1/2} \psi\left(\frac{x_1 \cos \theta + x_2 \sin \theta - b}{a}\right)$$

with $\mathbf{x} = (x_1, x_2) \in \mathbb{R}^2$, $b \in \mathbb{R}$ is the translation parameter, $a \in \mathbb{R}$ is the dilatation parameter and $\theta \in [0, 2\pi[$ is the direction parameter.

The function $\psi_{a,b,\theta}$ is oriented at the angle θ and is constant along lines $x_1 \cos \theta + x_2 \sin \theta = cst$. Transverse to these ridges it is a wavelet function. A basic tool for calculating Ridgelet coefficients is to view Ridgelet analysis as a wavelet analysis in the Radon domain. The Radon transform Rs can be obtained by applying the 1-D inverse Fourier transform to the 2-D Fourier transform restricted to radial lines going through the origin. This is the projection-slice formula that is used in image reconstruction from projection methods. The Ridgelet coefficients r_s of s are given by the 1-D wavelet transform to the projections of the Radon transform where the direction θ is constant and t is varying:

$$r_s(\theta, a, b) = \int_{\mathbb{R}} \psi_{a,b}(t) Rs(\theta, t) dt$$

2.2. Strategies for Discrete Ridgelet Transform

As we have seen, a basic strategy for calculating the continuous Ridgelet transform is first to compute the Radon transform Rs and secondly, to apply a 1-D wavelet transform to the slices $Rs(\theta, \cdot)$. The implementation of the discrete Ridgelet transform can use the same principle.

The discrete wavelet decomposition, associated to a filter bank,⁴ is easy to implement, is stable and invertible, and can be associated to a discrete orthogonal representation. The discretization of the Radon transform is more difficult to achieve. The majority of methods proposed in the literature have been devised for computerized tomography or to approximate the continuous formula.⁵⁻¹³ None of them, however, were specifically designed to be invertible transforms for discrete images and can therefore not be used for the discrete Ridgelet transform. The discrete Radon transform can be computed with a spatial strategy (summations of image pixels over a certain set of lines) or with a Fourier strategy:

1. Compute the 2-D Discrete Fourier Transform (DFT) of s
2. Extract Fourier coefficients along the lines L_θ going through the origin.
3. Compute the 1-D inverse DFT on each line L_θ (defined for each value of the angular parameter θ).

This approach can be problematic since step 2 is not naturally defined on discrete data. Recently, some articles studied the implementation of the discrete Ridgelet transform. Do and Vetterli proposed in² an implementation method of Ridgelet transform based on the use of the finite Radon transform. This method achieves both invertibility (the inverse transform is stable) and non-redundancy (the associated Ridgelet transform is orthogonal). This Radon transform integrates over lines, which are defined algebraically rather than geometrically, that can be rather arbitrarily spread out over the spatial domain. This approach is not based on a geometrically faithful notion of Ridgelets and suffers from artifacts (for example in denoising application: figure 3).

The team of Stanford proposed to use a scheme that substitutes the sampled values of the Fourier transform obtained on the square lattice with sampled values of \hat{s} on a polar lattice: the Fast Slant Stack described in.¹⁴ They use a pseudopolar Fourier domain. The discrete pseudopolar Fourier transform of a digital image is defined by sampling the 2-D Fourier transform at the collection of pseudopolar grid points.^{14, 15} For this, Donoho et

al. proposed in¹⁴ a fast pseudopolar Fourier transform based on a chirp-Z transform. The associated Radon transform (called Slant) is algebraically exact and geometrically faithful. However, the inverse transform requires an iterative approximation algorithm. The paper¹⁶ follows this strategy based on the pseudopolar grid. However, it uses a simple nearest-neighbor interpolation scheme to evaluate pseudopolar grid points in terms of nearby cartesian grid points.

In this paper, we propose to review the construction of a fast and simple reversible digital Ridgelet transform. For this, we use the Fourier strategy for the digital Radon transform. Our lines L_θ are defined with help of the discrete analytical geometry theory in the Fourier domain.^{17, 18} This solution allows us to have different Ridgelet decompositions according to the arithmetical thickness of the discrete lines. Our Radon backprojection is simple and permits an exact reconstruction. The objects defined in discrete analytical geometry (3D lines, planes, hyperplanes, ...) allow extensions to $3D^{19}$ and even higher dimensions.

3. 2-D DISCRETE ANALYTICAL RIDGELET TRANSFORM: DART

The idea behind our associated discrete Radon transform is to represent each direction by a discrete analytical straight line. For this we need a discrete straight line that has a central symmetry and that forms a “good” approximation of the corresponding Euclidean straight line (i.e. direction). This excludes the classical Bresenham discrete 2-D line.²⁰ Instead we chose discrete analytical 2D lines. It defines not a unique line but a family of lines with a thickness parameter, called arithmetical thickness. The arithmetical thickness provides a control over the transform redundancy factor and properties such as the connectivity of the straight line. The discrete line is analytically defined meaning that the discrete line is defined by equations that allow a precise study of the properties and immediate extensions to higher dimensions.

3.1. Definition and properties of the closed discrete analytical lines

The discrete analytical lines we use for our transform are defined as follows¹⁷:

$$L_{[p,q]}^\omega = \left\{ (x_1, x_2) \in Z^2 \mid |qx_1 - px_2| \leq \frac{\omega}{2} \right\}$$

with $[p, q] \in Z^2$ the direction of the Radon projection (we have $\theta = \arctan\left(\frac{q}{p}\right)$) and ω , a function of (p, q) , the arithmetical thickness. This definition is a variant to the discrete analytical lines introduced by J-P. Reveillès in 1991.¹⁸ It is easy to see that these discrete analytical lines $L_{[p,q]}^\omega$ have a central symmetry regardless of the value of ω . Moreover, the discrete analytical line definition can easily be extended to higher dimensions with the following formula: $|\sum_{i=1}^n q_i x_i| \leq \frac{\omega}{2}$.^{19, 21}

The arithmetical thickness ω is an important parameter that controls, among other things, the connectivity of the discrete line $L_{[p,q]}^\omega$: For $\omega < \max(|p|, |q|)$, the line is not connected ; for $\omega \geq \max(|p|, |q|)$, the line is 8-connected²¹ and for $\omega \geq |p| + |q|$, the line is 4-connected.²¹ These results are direct consequences of a well known result in discrete analytical geometry and more recent studies on discrete distances.^{17, 18} We have studied the Ridgelet transform with the naive lines ($\omega = \max(|p|, |q|)$, where $L_{[p,q]}^\omega$ is 8-connected), the pythagorean lines ($\omega = \sqrt{p^2 + q^2}$, where $L_{[p,q]}^\omega$ is 8-connected) and the supercover lines ($\omega = |p| + |q|$, where $L_{[p,q]}^\omega$ is 4-connected).

3.2. Definition of the discrete analytical Radon transform

We use the Fourier domain for the computation of our discrete Radon transform: Fourier coefficients of \hat{s} are extracted along the discrete analytical line $L_{[p,q]}^\omega$ (the extracted points of the line are ordered in a natural way):

$$P_{[p,q]}^\omega = \bigcup_{k \in Z^+} \hat{s}(f_1^k, f_2^k) \text{ with } |qf_1^k - pf_2^k| \leq \frac{\omega}{2}$$

and we take the 1-D inverse discrete Fourier transform of $P_{[p,q]}^\omega$ on each value of the direction $[p, q]$. This straightforward transform requires the computation of the inverse Fourier transform for non-equispaced grid points (the sampling of the Fourier coefficients depends of the type of discrete analytical line). The direct evaluation

of this inverse Fourier transform takes $O(N^2)$ arithmetical operations, too much for practical purposes. Several methods were introduced in the literature for the fast computation of an approximation Fourier transform for nonequispaced data or for the computation of the polar Fourier transform^{5, 7, 8, 11, 22} but none of them were specifically designed to be invertible. In,^{14, 15, 23} an iterative approach is proposed to find an inverse and the authors showed that the error reconstruction tends to machine precisions. We want to define a discrete Ridgelet transform (consequently a Radon transform) which is fast, simple and associated to an exact reconstruction. By using discrete analytical lines, by definition for a given arithmetical thickness, we consider the best discrete approximation of the Euclidean line for each line direction and we use a classical discrete inverse Fourier Transform defined for equispaced data (as in¹⁶).

At last, the set of discrete directions $[p, q]$ for a complete representation has to be determined. The set of line segments must cover all the square lattice in the Fourier domain. For this, we define the directions $[p, q]$ according to pairs of symmetric points from the boundary of the 2-D discrete Fourier spectra. Notice that this set of angles is not equispaced. This strategy also the one followed by Stanford.^{14, 16}

PROPOSITION 3.1. *Let a square lattice be defined as $\Omega_N^2 = [-N; N] \times [-N; N]$. Let us consider the set of directions (p_m, q_m) with $0 \leq m \leq 2N$, $(p_m, q_m) = (N, m - N)$ and for $2N + 1 \leq m \leq 4N - 1$, $(p_m, q_m) = (3N - m, N)$. The set of all discrete analytical lines defined by $|q_m f_1 - p_m f_2| \leq \frac{\omega_m}{2}$ with $\omega_m \geq \sup(|p_m|, |q_m|)$ provides a complete cover of the lattice Ω_N^2 .*

The proof of this proposition is obvious since we are dealing here with discrete lines that are at least 8-connected as stated in the previous section. As soon as we take $\omega = \sup(|p_m|, |q_m|) - 1$ the lattice is not covered anymore (because of $L_{[0,1]}^{\sup(|p_m|, |q_m|) - 1 = 0}$ and $L_{[1,0]}^0$). Other strategies that provide a complete cover and a lower redundancy are under investigation. This is still an open and somewhat difficult question. In our applications we chose to work only with connected discrete lines.

The shape of the discrete lines and the cover of the Fourier domain depend on its arithmetical thickness:

- The closed naive lines provide a relatively small Radon redundancy factor of ≈ 2.05 . These lines are better suited for applications such as partial reconstruction where a relatively small redundancy is an asset.
- The supercover lines provide a more important Radon redundancy factor of ≈ 3.05 . These lines are well suited for applications such as denoising.
- The pythagorean lines provide an intermediate Radon redundancy factor of ≈ 2.35 .

The indicated redundancy factor, computed by experimentations, is a mean average for each type of lines as this factor depends of the dimension of the image.

3.3. Inversion of the discrete analytical Radon transform

We now briefly discuss the strategy for inverting our discrete Radon Transform:

1. Compute the 1-D DFT transform for each set $R^\omega s([p, q], \cdot)$ to obtain $P_{[p,q]}^\omega$
2. For all the directions $[p, q]$, substitute the sampled value of \hat{s} on the lattice where the points fall on lines $L_{[p,q]}^\omega$ with the sampled value of \hat{s} on the square lattice:

$$\hat{s}^{[p,q]}(f_1^k, f_2^k) = P_{[p,q]}^\omega(k) \text{ such that } |qf_1^k - pf_2^k| \leq \frac{\omega}{2}$$

for $0 < k < \text{length of } L_{[p,q]}^\omega$.

Due to the redundancy, some Fourier coefficients belong to more than one discrete line. In this case, the Fourier value is defined by the mean average*.

3. Apply the 2-D IDFT transform.

The previous procedure allows us to obtain an exact reconstruction.

*The number of times a pixel (f_1, f_2) belongs to a discrete line depends of the frequency (it is more important at low frequencies) and depends of the type of discrete lines.

3.4. Definition of the DART

Now, to obtain the Ridgelet transform, we take a 1-D wavelet transform along the radial variable in Radon space. The choice of discrete one-dimensional wavelet transform is discussed by Starck et al. in.¹⁶ They indicate that experience has shown that compactly-supported wavelets can lead to many visual artifacts when used with nonlinear processing. The choice of the type of 1-D wavelet transform depends of the goal of the transform. In this study, we use time filters (D20 filters) that have very large supports. If the same experiments are done with too small filters, the denoised image will contain some disturbing artifacts.

In order to illustrate the function associated with our DART, we apply the DART inversion of a point. The figure 1a illustrates the influence of the wrap-around artifacts. From the figures 1b and 1c, we see that our DART is associated to the correct Ridge function: the function $\psi_{a,b,\theta}$ is oriented at the angle θ , is constant along lines and it is a wavelet function transverse to these ridges.

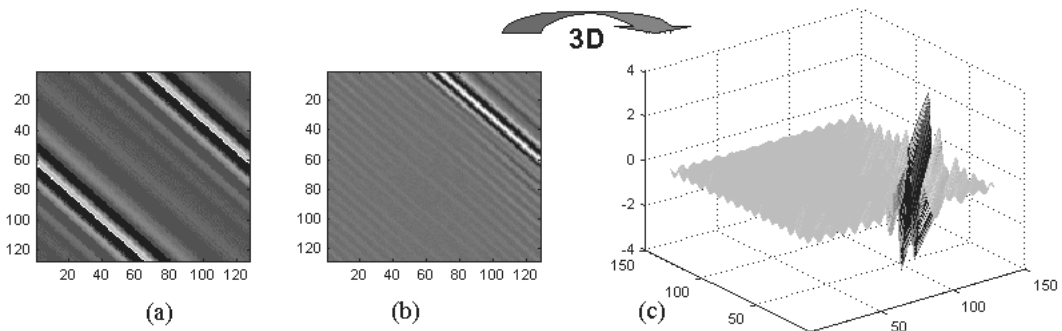


Figure 1. The DART backtransform of a point : (a) using the closed naive lines without zeropadding strategy (b) using the closed naive lines and zeropadding strategy (c) the 3-D surface of the DART function

4. DENOISING WITH THE 2D-DART

The denoising procedure by Ridgelet transform simply consists in thresholding the Ridgelet coefficients and computing the inverse Ridgelet transform. The thresholding is performed with the help of an undecimated method (UDWT) developed for the Daubechies D20 wavelet scale 4 decomposition. Let r_f be the noisy undecimated Ridgelet coefficients, we use the following hard-thresholding:

$$r_f(a, b, \theta) = \begin{cases} r_f(a, b, \theta) & \text{if } |r_f(a, b, \theta)| \geq \alpha\sigma \\ 0 & \text{otherwise} \end{cases} \quad (1)$$

α can be defined as $\alpha = \sqrt{2 \log(N)}$, and the variance σ is estimated using the absolute median of the wavelet decomposition's first scale of each radial projection.²⁴

The redundancy of the wavelet decomposition, associated with this method, reduces artifacts that appear after thresholding.

We can generalize to color images the discrete wavelet decomposition. For this, we apply convolutions on the three components of the color image. With the same strategy, we can compute the Radon transform on the three components. But we must select an adapted color space. For the denoising application, we choose the $Y C_r C_b$ space, to treat separately the color and intensity components.

In order to study precisely the result of the denoising algorithm with different types of discrete analytical lines we have generated an artificial noisy image by adding important white noise. This example illustrates the results for different definition of the lines $L_{p,q}^D$. We see in the figure 2 that the features are generally correctly reconstructed and the noise is smoothed. But if we study more precisely the result on the woman's hat, we see

that the denoising is better for $D = \frac{|p|+|q|+1}{2}$ than for $D = \frac{\max(|p|,|q|)}{2}$. The first choice of D introduces more redundancy into the decomposition and thus reduces artifacts. As in the wavelet decomposition, overcompleteness provides advantages for denoising.



Figure 2. (a) noisy image woman (b) denoised by ridgelet decomposition with $D = \frac{\max(|p|,|q|)}{2}$ (c) denoised by ridgelet decomposition with $D = \frac{|p|+|q|+1}{2}$

In order to obtain the image denoising results presented in this paper, we propose to use the discrete Radon transform defined with naive lines. This choice indeed corresponds to the faster algorithm of our proposed methods. Moreover, it corresponds to the less redundant reconstructible decomposition and will be associated to inferior performance since the overcompleteness provides advantages for denoising.

We briefly compare the DART with the other Ridgelet transform implementations we know about. Figure 3 considers the Mandrill image, and compares the denoising of this image by thresholding the different Ridgelet transforms and undecimated wavelet transform. We use the SNR and the visual analysis to measure the performance. We observe that :

- The Ridgelet based on the Fast Slant Stack transform[†] (Beamlab code) and the DART reconstruction does not contain the many blemishes that one sees in the wavelet reconstructions. The SNR measures of these two transforms are better. But we have parasitic lines present in the Ridgelet reconstruction due to the selection of an important contour in an area of the image.
- The Do's Ridgelet transform corresponds to a critical sampling. The reconstruction associated with a nonlinear processing contains thus many visual artifacts.
- The Stanford reconstruction and DART reconstruction are very similar (with this denoising strategy). Notice that the number of parasitic lines is inferior in the DART reconstruction.

The DART can be easily extended to a local transform by a smooth partitioning: the image is smoothly windowed into squares; Analyse each square by the DART. As in the Ridgelet transform, the denoising by Local transform consists simply in thresholding the Local Ridgelet coefficients and computing the inverse transform. The local Ridgelet Transform is used to introduce redundancy in 2-D image restorations and to process locally 2-D image contours. For this decomposition, the analysis is better localized in the spatial domain. This property eliminates the parasitic lines present in the Ridgelet reconstruction due to the selection of an important contour in an area of the image.²⁵

To illustrate the local DART transform based on discrete analytical lines, we apply the local Dart on the Mandrill example. We observe that the Local DART enjoy superior performance over the DART transform. For this decomposition the analysis is better localized in the spatial domain. This property eliminates the parasitic lines present in the DART reconstruction and due to the selection of an important contour in an area of the image. As for the Ridgelet transform, we can use other definitions of discrete analytical lines for Local DART.

[†]In this case, we use undecimated D20 wavelets and the local variance is estimated using the absolute median of the wavelet decomposition's first scale of each radial projection.

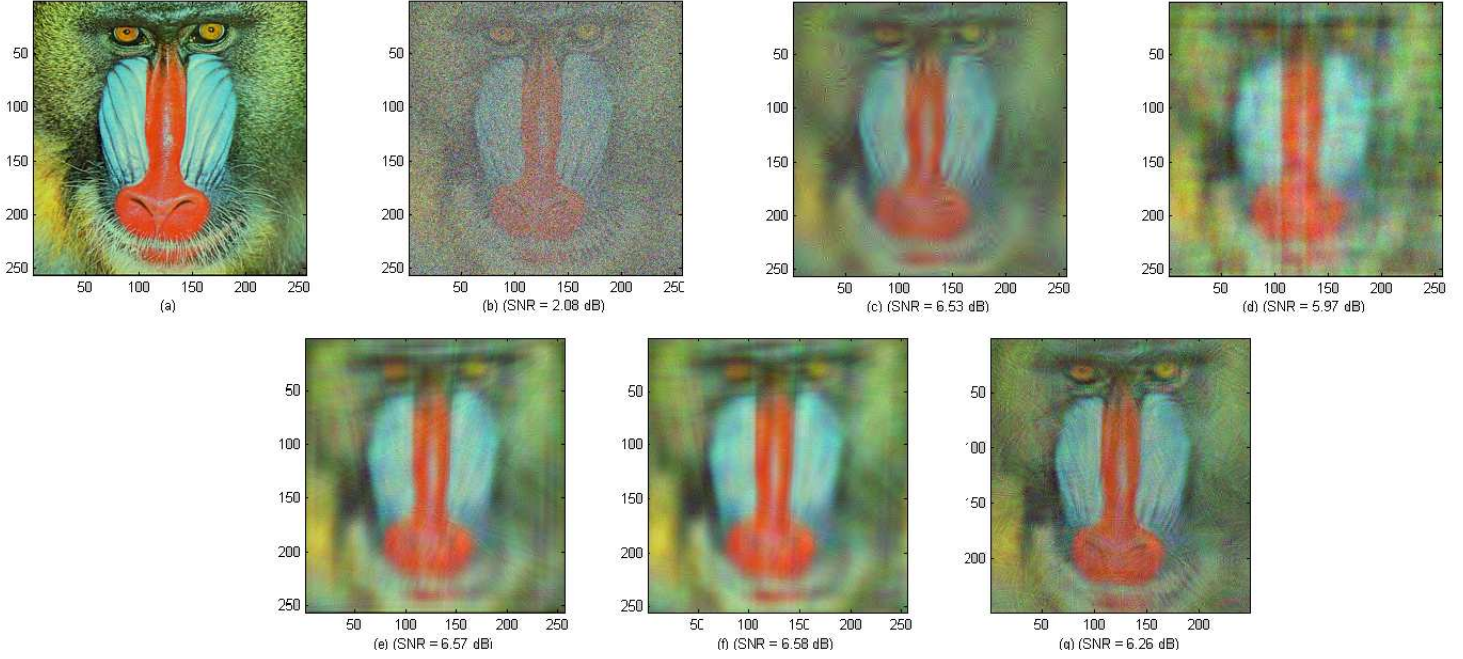


Figure 3. (a) Original image (b) Noisy image (c) denoising with the undecimated wavelet transform (d) denoising with the Do and Vetterli orthogonal Ridgelet (e) denoising with the Ridgelet based on the Fast Slant Stack transform and undecimated D20 wavelets (f) denoising with the DART based on Naive lines and undecimated D20 (g) denoising with the local-DART based on Naive lines and undecimated D20 wavelets

We have developed an another example of denoising algorithm (Figure 4). Notice that the Do's Ridgelet transform is not illustrated because the image matrix must be of size P by P , P a prime number. These experiments confirm that the Stanford reconstruction and DART reconstruction are very similar. However, as we have said, the backprojection DART algorithm is simpler and the DART representation is more flexible (with the variable line thickness).

5. THE 3-D RIDGELET TRANSFORM

Now, we present the extension of the 2-D discrete strategy to the 3-D space to define a reversible 3-D discrete Ridgelet transform. Preliminary results of this study are presented in.^{26, 27}

5.1. The 3-D continuous Ridgelet Transform

The Ridgelet transform of $f \in L^2(R^3)$ [‡] can be extended to 3-D case by:

$$r(a, b, \theta, \gamma) = \int_{R^3} \overline{\psi}_{a,b,\theta,\gamma}(\mathbf{x}) f(\mathbf{x}) d\mathbf{x} \quad \text{with } \mathbf{x} = (x_1, x_2, x_3) \quad (2)$$

The Ridgelet 3-D function $\psi_{a,b,\theta,\gamma}$ is defined from a wavelet 1-D function ψ , $b \in R$ is the translation parameter, $a \in R^{*+}$ is the dilatation parameter and $\theta \in [0, 2\pi[$, $\gamma \in [0, \pi[$ are the direction parameters:

$$\psi_{a,b,\theta,\gamma}(x_1, x_2, x_3) = \psi\left(\frac{x_1 \cos \theta \cos \gamma + x_2 \sin \theta \cos \gamma + x_3 \sin \gamma - b}{a}\right) \quad (3)$$

[‡] $f \in L^2(R^3)$ if $\int_{R^3} \|f(x_1, x_2, x_3)\|^2 dx_1 dx_2 dx_3 < \infty$



Figure 4. (a) Original image (b) Noisy image (c) denoising with the undecimated wavelet transform (d) denoising with the Ridgelet based on the Fast Slant Stack transform and undecimated D20 wavelets (e) denoising with the DART based on Naive lines and undecimated D20 (f) denoising with the local-DART based on Naive lines and undecimated D20 wavelets

The function $\psi_{a,b,\theta,\gamma}$ is oriented at the angles θ and γ and is constant along lines:

$$x_1 \cos \theta \cos \gamma + x_2 \cos \theta \sin \gamma + x_3 \sin \theta = cst. \quad (4)$$

As for the 2-D case, a basic tool to calculate Ridgelet coefficients is to view the Ridgelet analysis as a wavelet analysis in the Radon domain. The Ridgelet coefficients r_f of f are given by the 1-D wavelet transforms on projections of the Radon transform R_f where the directions θ, γ are constant and t is varying.

The 3-D continuous Radon transform can be defined using 1-D projections of a 3-D object f where these projections are obtained by integrating f on a plane.²⁸ The 3-D continuous Radon transform of an object is related to its 3-D Fourier transform via the central slice theorem:

$$R_f(t, \theta, \gamma) = \int_R \widehat{f}(\xi \cos \theta \cos \gamma, \xi \cos \theta \sin \gamma, \xi \sin \theta) e^{j\xi t} d\xi \quad (5)$$

with \widehat{f} the 3-D Fourier transform of f .

6. THE 3-D DISCRETE ANALYTICAL RADON TRANSFORM

6.1. Principles of the 3-D discrete Radon transform

As we have seen, a basic strategy to calculate the ridgelet transform is first to compute the Radon transform R_f and secondly, to apply a 1-D wavelet transform to the slices $R_f(., \theta, \gamma)$. The discrete procedure uses the same principle.

The discretization of the 3-D Radon transform is the extension of the 2-D discrete Radon transform method: we compute the 3-D Discrete Fourier Transform of f , we extract Fourier coefficients that belong to straight lines $L_{\theta, \gamma}$ going through the origin, and we compute the 1-D Discrete Fourier Transform on each line $L_{\theta, \gamma}$ (defined for each value of the two angular parameters).

The idea is to represent each direction with an analytical 3-D discrete straight line in the Fourier domain.

As for the 2-D case, since none of the "classical" notions of discrete 3-D lines fits all of these conditions, we propose our own families of discrete 3-D lines with help of the discrete analytical geometry.

In this paper we review one method to define 3-D discrete lines covering all 3-D cubic lattice: Cover the 3-D cubic lattice by the extrusion 2-D discrete lines. A another method is proposed in.²⁷

6.2. Extrusion of discrete 2-D analytical lines

The idea is to use properties of covering results that we have in 2-D to define discrete 3-D lines preserving these properties: cover the 3-D cubic lattice with a specific set of 3-D planes and each discrete plane is then being covered with a set of 2-D line segments.

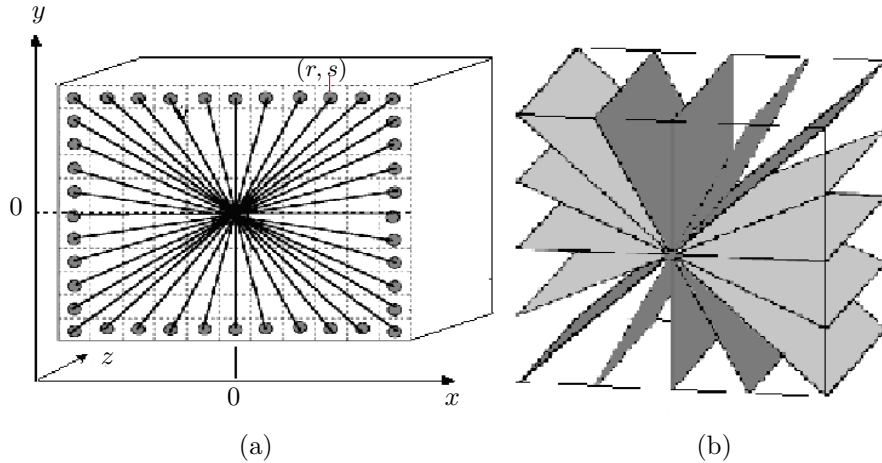


Figure 5. (a) Choice of the discrete discrete lines $L_{[r,s]}^{\omega_P}$ (b) cover of the 3-D Fourier domain with euclidian planes

To compute a discrete plane $P_{[r,s]}^{\omega_P}$ for our application,²⁹ we need to define the analytical 2-D discrete line $L_{[r,s]}^{\omega_P} = \{(x, y) \in Z^2 \mid |rx + sy| \leq \frac{\omega_P}{2}\}$ and the discrete plane is obtained by the extrusion of the analytical 2-D discrete line along the z-axis (the central plane axis is chosen arbitrarily).

Then, the 3-D cubic lattice is covered with discrete analytical 3-D planes defined by the following equation (figure 5):

$$P_{[r,s]}^{\omega_P} = \left\{ (x, y, z) \in Z^3 \mid |sx - ry + 0 \cdot z| \leq \frac{\omega_P}{2} \right\} \quad (6)$$

where $(r, s) \in Z^2$ are the γ direction of the plane and ω_P , function of r and s , is the arithmetical thickness. These planes have a central symmetry and are the analytical discretization of the Euclidean planes $P_\gamma : sx - ry + 0 \cdot z = 0$ for a given arithmetical thickness w_P .

We extract Fourier coefficients from $P_{[s,r]}^{\omega_P}$ and we cover this 2-D domain $\Phi_{U,V}$ with discrete 2-D analytical lines $L_{[p,q]}^{\omega_L} = \{(u, v) \in Z^2 \mid |pu + qv| \leq \frac{\omega_L}{2}\}$ with (p, q) are the θ direction (this discrete 3-D line can be viewed as intersection of two orthogonal discrete planes).

At last, the set of discrete directions $[p, q]$ (associated with the lines) and $[r, s]$ (associated with the planes) for a complete representation has to be determined. The set of 3-D line segments must cover all the cubic lattice in the Fourier domain. It has been shown that 2-D lines $|px + qy| \leq \frac{\omega_L}{2}$ chosen according to pairs of symmetric points from the boundary of the 2-D discrete Fourier spectra (as in figure 5a) cover the 2-D Fourier domain when the arithmetical thickness verifies $\omega_L \geq \max(|p|, |q|)$.

In order to cover all the cubic lattice in the Fourier domain, we thus define the directions according to pairs of symmetric points from the boundary of:

- the plane $\{z = 0\}$ for the planes $P_{[r,s]}^{\omega_P}$.
- the plane $P_{[r,s]}^{\omega_P}$ for the lines $L_{(p,q)}^{\omega_L}$.

According to the 2-D domain, the 3-D Fourier domain is always covered by the analytical 3-D discrete lines if $\omega_P \geq \max(|r|, |s|)$ and $\omega_L \geq \max(|p|, |q|)$.

Now, we can use the Fourier domain for the computation of our discrete Radon transform. For this, Fourier coefficients of \hat{f} are extracted along the proposed 3-D discrete analytical lines and ordered in a natural way and we take the 1-D inverse discrete Fourier transform on each value of the direction.

The sampling of the extracted Fourier coefficients depends on the 3-D discrete analytical lines used to compute the discrete Radon transform. As for the 2-D case, we consider that the 3-D discrete analytical lines are a good approximation of the Euclidian lines for each line direction and we use a classical discrete Fourier transform defined for equispaced coefficients.

For the Ridgelet transform, we must take a 1-D wavelet transform along the radial variable in Radon space. In this article, we illustrate the 3-D Ridgelet transform with denoising applications. We thus propose to use an undecimated wavelet transform.

6.3. Reconstruction of the 3-D discrete Radon transform

Our analytical reconstruction procedure works as follows:

1. Compute the 1-D Fourier transform for each set $R_f(., \Theta, \gamma)$;
2. Substitute the sampled value of \hat{f} on the lattice where the points fall on 3-D discrete lines with the sampled value of \hat{f} on the cubic lattice;
3. Apply the 3-D inverse Fourier transform.

The 3D DART followed by its inverse provides an exact reconstruction properties if the set of directions of lines provides a complete cover of the cubic lattice. The 3-D Fourier domain is always covered by the analytical 3-D discrete lines for all the presented thickness ($\omega(p, q) \geq \max(|p|, |q|)$). This transform is thus always perfectly revertible.

6.4. Redundancy of the 3-D Discrete Analytical Ridgelet Transform

The redundancy factor of 3-D DART representation depends on the 3-D discrete analytical lines used to define the Discrete Radon transform and the type of wavelet transform. As stated, the thickness parameters allow us to control the redundancy factor of the transform and to adapt it to a given application. Table 1 shows the different redundancy factor, computed by experimentation, in function of the discrete Radon transform strategies and the object thicknesses.

Table 1. Discrete Radon transform redundancy table

Discrete objets thicknesses	naive	pythagorician	supercover
3-D discrete planes and 2-D discrete lines	3.9	4.9	9.7

As for the two discrete Radon transform strategies, the voxels covering low frequencies in the Fourier domain belong to more discrete lines than those covering the higher frequency. The redundancy is concentrated mainly in low frequencies.

The 3-D DART can be easily extended to a local transform by the smooth partitioning windowed into cubes. Each cube is analysed by the DART.

7. DENOISING APPLICATIONS

In order to obtain the videos denoising results presented in this paper, we propose to use the discrete Radon transform defined with naive planes and 2-D discrete naive lines. This choice indeed corresponds to the faster algorithm of our proposed methods. Moreover, it corresponds to the less redundant reconstructible decomposition and will probably associated to inferior performance since the overcompleteness provides advantages for denoising.

The first video is a sequence of 279 images of size (351×281) with their three-colour components (figure 6 (a)). It comes from the Video Quality Experts Group (V.Q.E.G.). A Gaussian noise is added to the three-colour components of the video ($\sigma = 70$). The colour video is decomposed into three videos corresponding to the three-colour components. We independently denoise every component with the associated 3-D local Discrete Analytical Ridgelet Transform and we reconstruct the video with the inverse 3-D local-DART. The local denoising processing is applied to blocks of size $(71 \times 71 \times 71)$.

We have studied the colour video denoising with the DART in several classical colour spaces :

- Red, Green and Blue : the most used in colour image processing because of material dependance,
- Hue, Saturation and Value : colour representation with separated components more subjective,
- Y (luminance), Cb (blue chrominance) and Cr (red chrominance) : international standard dedicated image digital coding,
- XYZ : correct some RGB defaults, the Y component is considered as the luminance of the incident spectra,
- Principle Components Analysis : projection of the voxel colour on the factoriel axis.

First studies have showed that RGB and YCbCr spaces are the good colour representation for video denoising with the 3-D DART.

We can see in figure 6 that the quality of colours and linear forms perception are very encouraging for the colour video denoising: colours in the video after the denoising are not debased. The rectilinear contours are maintained and not distorted. Futhermore, we correctly restore zones containing small objects. The 3-D DART allows to process the temporal evolution like contours.

Now, we propose to evaluate the robustness of our method with very noisy data. This second video is a sequence of 279 images of size (279×279) with their three-colour components (figure 7 (a)). It comes from the Video Quality Experts Group (V.Q.E.G.). A very important Gaussian noise ($\sigma = 264$) is added to the three-colour components of the video.

With very noisy data, the denoising results (figure 7c) are correct with regard to the noisy video: colours and contours of the differents animals are correctly restored. But with this level of noise, the calendar numbers are difficultly visible.

8. CONCLUSION

So far, the development of the 2-D discrete Ridgelet transform has been investigated by two teams in previous works. In this paper, we have reviewed an implementation of the 2-D/3-D Ridgelet transform. Our innovative choice is to use the formalism of the discrete analytical geometry theory in the Fourier domain, in order to define a new discrete Ridgelet transform: the Discrete Analytical Ridgelet Transform (DART).

The DART algorithm is easy to implement. It provides an exact reconstruction property: the DART followed by a reverse DART is a one-to-one transform. Our experiments have shown that our approach presents a limited wrap-around effect, that does not influence the denoising results. Moreover, by using the analytical formalisation, we define a flexible Ridgelet transform: we can define different DART decompositions according to the arithmetical thickness of the analytical discrete lines.

We have extended the Ridgelet Transform to 3-D by using the formalism of the discrete analytical geometry theory. In this paper, we have illustrated one strategy to implement the 3-D Discrete Analytical Ridgelet Transform: 3-D planes covered with 2-D line segments.

We have illustrated the performances of the DART for denoising problems with Gaussian noise. This study indicates that the DART and the Local-DART thresholding are outstanding in the 2-D/3-D image denoising and enable an effective denoising of a colour video, even with very noisy videos.

This work can be extended to several directions. One of the theoretical questions in discrete geometry is the problem of defining an arithmetical thickness function that provides a smaller redundancy and a cover of the Fourier domain. This is still an open and difficult arithmetical problem. One of the most important interests of the discrete analytical approach is the possibility to easily extend our work to n-D (we are investigating the application of a 4D DART to the denoising process of animated 3-D images). We propose to extract the Fourier coefficients along a n-D discrete analytical line going through the origin. The principle of the n-D method is the same as in the 3-D case with the same properties (exact reconstruction, rapidity, flexible definition). The choice of colour basis for the denoising problematic remains an opened problem through.

REFERENCES

1. E. Candès, *Ridgelets: Theory and Applications*. PhD thesis, Dpt of Statistics, Stanford University, <http://www.acm.caltech.edu/emmanuel/>, August 1998.
2. M. Do, *Directional Multiresolution Image Representations*. PhD thesis, Department of Communication Systems, Swiss Federal Institute of Technology Lausanne, November 2001.
3. A. Flesia, H. Hel-Or, A. Averbuch, E. Candès, R. Coifman, and D. Donoho, "Digital implementation of ridgelet packets," in *Beyond Wavelets*, J. Stoeckler and G. V. Welland, eds., Academic Press, 2002.
4. S. Mallat, "A theory for multiresolution signal decomposition : the wavelet transform," *IEEE Trans. on PAMI* **11**, pp. 674–693, 1989.
5. M. Bronstein, A. Bronstein, and M. Zibulevsky, "Applications of non-uniform fft for acoustic diffraction tomography," tech. rep., <http://visl.technion.ac.il/bron/works>, march 2002.
6. J. Fessler and B. Sutton, "A min-max approach to the multidimensional nonuniform fft: Application to tomographic image reconstruction." To be Published in *IEEE Trans. on Signal Processing*, 2001.
7. K. Fourmont, "Non-equispaced fast fourier transforms with applications to tomography," tech. rep., Math Department at the University of Muenster, <http://www.math.uni-muenster.de>, May 2002.
8. F. Natterer, "Numerical methods in tomography," *Acta Numerica*, 1999.
9. D. Potts and G. Steidl, "A new linogram algorithm for computerized tomography," *IMA Journal of Numerical Analysis* **21**, pp. 769–782, 2001.
10. J. Roerdink and M. Westenberg, "Data-parallel tomographic reconstruction: a comparison of filtered back-projection and direct fourier reconstruction," *Parallel Computing* **24**, pp. 2129–2144, 1998.
11. P. Toft, *The Radon Transform: theory and implementation*. PhD thesis, Dpt of Mathematical Modelling, Technical University of Denmark, 1996.
12. M. Brady, "A fast discrete approximation algorithm for the radon transform," *SIAM J. Computer* **27**, pp. 107–119, February 1998.



Figure 6. Extracting of four images issued: (a) original colour video, (b) noisy colour video and (c) colour video denoised with the 3-D DART in RGB space

13. F. Matús and J. Flusser, "Image representation via a finite radon transform," *IEEE Trans. on Pattern Analysis and Machine Intelligence* **15**(10), pp. 996–1006, 1993.
14. A. Averbuch, R. Coifman, D. Donoho, M. Israeli, and J. Walden, "Fast slant stack: A notion of radon transform for data in a cartesian grid which is rapidly computible, algebraically exact, geometrically faithful and invertible," *SIAM Scientific Computing to appear*, 2001.
15. Y. Shkolnisky, A. Averbuch, and D. Donoho, "2d fourier based discrete radon transform," submitted, Dpt of Statistics, Stanford University, <http://www.math.tau.ac.il/~amir1/publications.html>.
16. J.-L. Starck, E. Candès, and D. Donoho, "The curvelet transform for image denoising," *IEEE Transactions on Image Processing* **11**, pp. 670–684, November 2002.

17. E. Andres, "Modélisation analytique discrète d'objets géométriques." Habilitation, Université de Poitiers, 2000.
18. J.-P. Reveillès, "Géométrie discrète, calcul en nombres entiers et algorithmique." Habilitation, Université Louis Pasteur de Strasbourg, 1991.
19. P. Carré, D. Helbert, and E. Andrés, "3-d fast ridgelet transform," in *ICIP'03, IEEE International Conference on Image Processing*, (Barcelona, Spain), September 2003.
20. J. Bresenham, "Algorithms for computer control of a digital plotter," *IBM Sys. Journal* **4**, pp. 25–30, January 1965.
21. E. Andres, R. Acharya, and C. Sibata, "Discrete analytical hyperplanes," *Graphical Models and Image Processing* **59**(5), pp. 302–309, 1997.
22. D. Potts, G. Steidl, and M. Tasche, "Fast fourier transforms for nonequispaced data: a tutorial," in *Modern Sampling Theory: Mathematics and Applications*, 2001.
23. A. Averbuch and Y. Shkolnisky, "3d discrete x-ray transform," submitted, <http://www.math.tau.ac.il/~amir1/publications.html>.
24. D. Donoho, "Wavelet shrinkage and W.V.D. : a 10-minute tour," tech. rep., Stanford University, 1992.
25. J.-L. Starck, E. Candès, and D. Donoho, "the curvelet transform for image denoising," *IEEE Trans. Image Processing* **11**, pp. 131–141, june 2002.
26. D. Helbert, P. Carré, and E. Andres, "La transformée ridgelet analytique discrète 3D," in *GRETSI*, (Paris, France), september 2003.
27. P. Carré, D. Helbert, and E. Andres, "3D fast ridgelet transform," in *ICIP*, (Barcelona, Spain), september 2003.
28. A. Averbuch and Y. Shkolnisky, "3d Fourier based discrete Radon transform," *Applied and Computational Harmonic* **15**, pp. 33–69, 2003.
29. E. Andres, R. Acharya, and C. Sibata, "Discrete analytical hyperplanes.," *CVGIP: Graphical Model and Image Processing* **59**(5), pp. 302–309, 1997.

